



STRUCTURAL SCIENCE
CRYSTAL ENGINEERING
MATERIALS

Volume 75 (2019)

Supporting information for article:

**A further investigation of the complex M3 murataite structure using
Hf substitution and STEM-EELS techniques**

Ryosuke S. S. Maki and Peter E. D. Morgan

Table S1. Powder diffraction lines for murataite minerals at $2\theta = 10\text{--}50^\circ$.

hkl	Adams et al. (1974) a		Portnov et al. (1981) b		Ercit & Hawthorne (1995) c	
	I	d _{exp.}	I	d _{exp.}	I	d _{exp.}
111	30.0	8.51			46.8	8.5944
200	10.0	7.38			24.8	7.4430
220	5.0	5.25			4.0	5.2630
311	5.0	4.46			2.3	4.4883
222	5.0	4.29			2.1	4.2972
400	5.0	3.708			2.6	3.7215
331	10.0	3.414			6.9	3.4151
420	5.0	3.314			0.9	3.3286
422	10.0	3.028	10.0	3.01	5.4	3.0386
333, 511 d	100.0	2.858	100.0	2.86	100.0	2.8648
440	5.0	2.622			1.6	2.6315
531					0.4	2.5162
600, 442 d	60.0	2.468	40.0	2.48	20.7	2.4810
620					0.4	2.3537
533	10.0	2.265			4.7	2.2701
622					0.5	2.2442
444	20.0	2.141	10.0	2.13	7.2	2.1486
711, 551	20.0	2.080	10.0	2.08	7.7	2.0845
640	10.0	2.058			4.0	2.0643
642	5.0	1.981			0.9	1.9892
731, 553	5.0	1.933	10.0	1.94	0.9	1.9380

Ideal formula, Lattice constant (\AA)a $(\text{Na}, \text{Y}, \text{Er})_4(\text{Zn}, \text{Fe})_3(\text{Ti}, \text{Nb})_6\text{O}_{18}(\text{F}, \text{OH})_4$, $a = 14.863(5)$ \AA b $(\text{Na}_{1.89}\text{Y}_{1.81}\text{Yb}_{0.04}\text{Fe}_{0.32})_{4.06}(\text{Zn}_{1.98}\text{Ca}_{1.19})_{3.17}\text{Ti}_6\text{O}_{19.19}$, $a = 14.87(2)$ \AA c $(\text{Y}, \text{Na})_6(\text{Zn}, \text{Fe})_5\text{Ti}_{12}\text{O}_{29}(\text{O}, \text{F})_{10}\text{F}_4$, $a = 14.886(2)$ \AA d For the two strongest lines, all (hkl) are divisible by 3 for the sub-cell - this was missed or insufficiently clear in the original PXRDs.

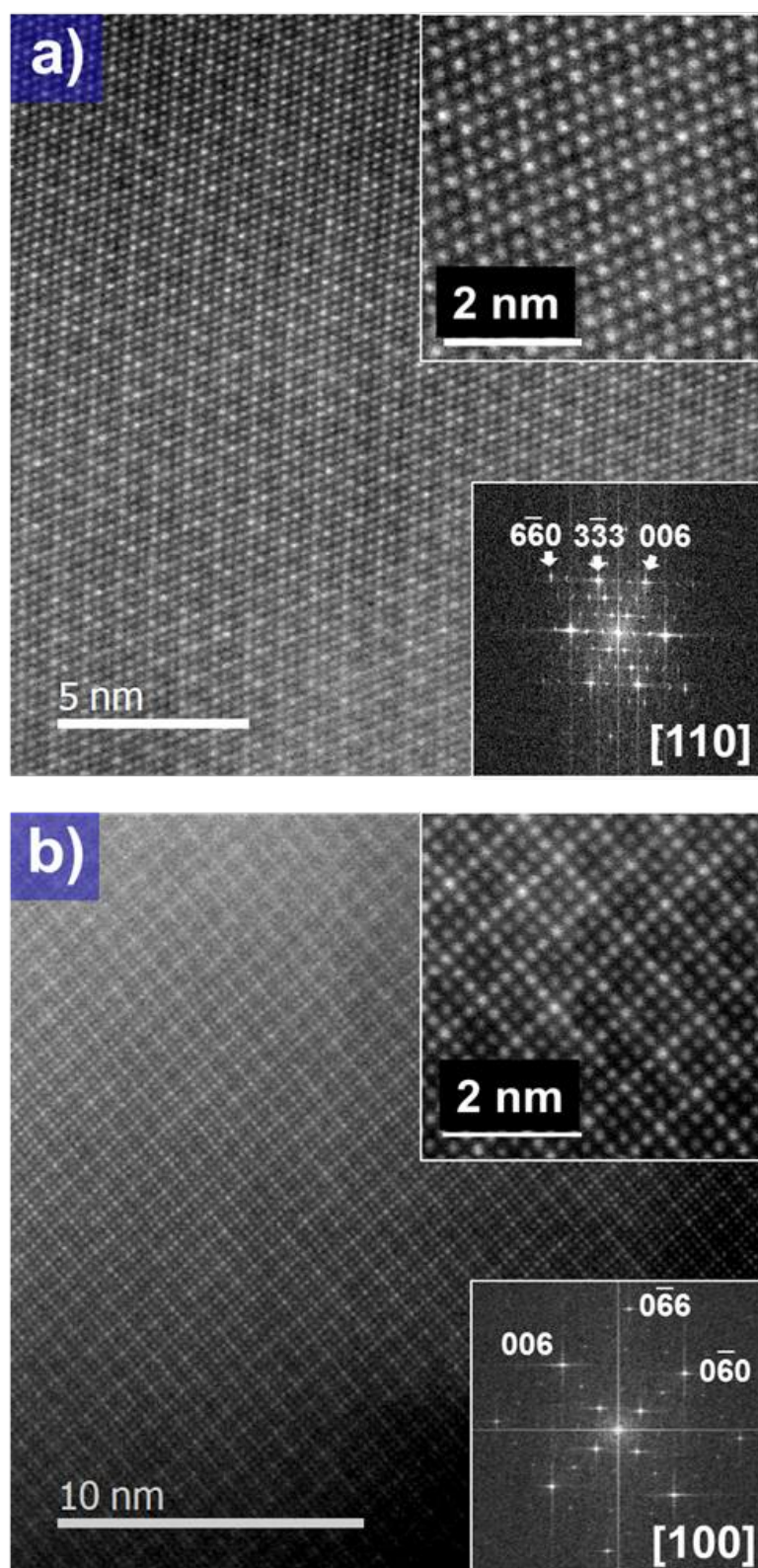


Fig. S1. The HAADF-STEM images (a) in (110) plane and (b) the (100) plane of the CMTZAF sample. The FFT patterns in the (110) and (100) planes of the reciprocal lattice are shown inset. The

$3 \times 3 \times 3$ fluorite-type superstructure, M3, forms and well crystalizes easily because of a liquid phase (under study) which develops on heating up.

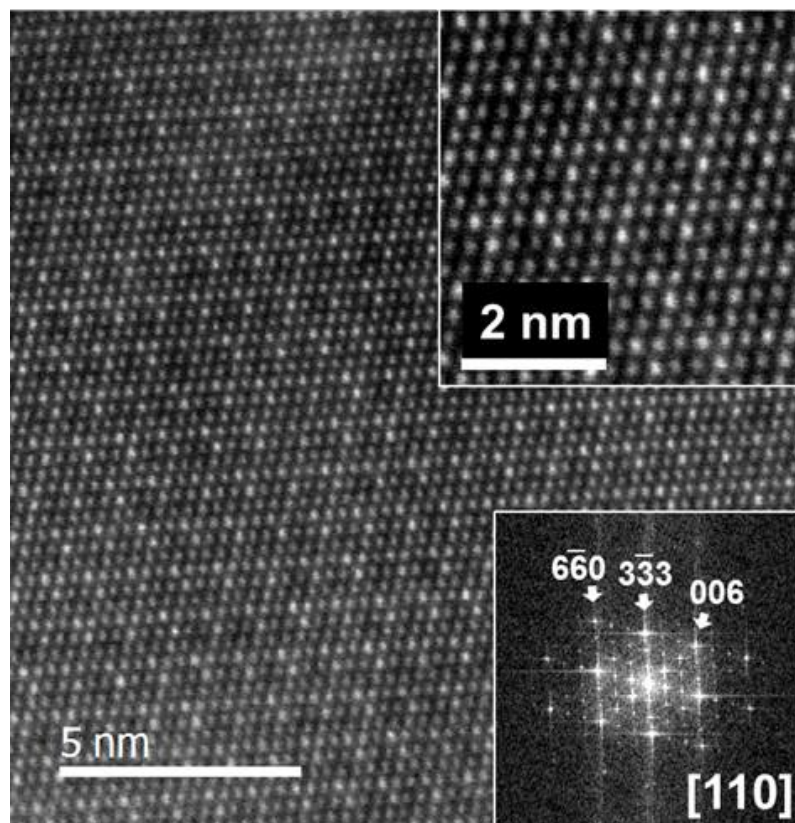
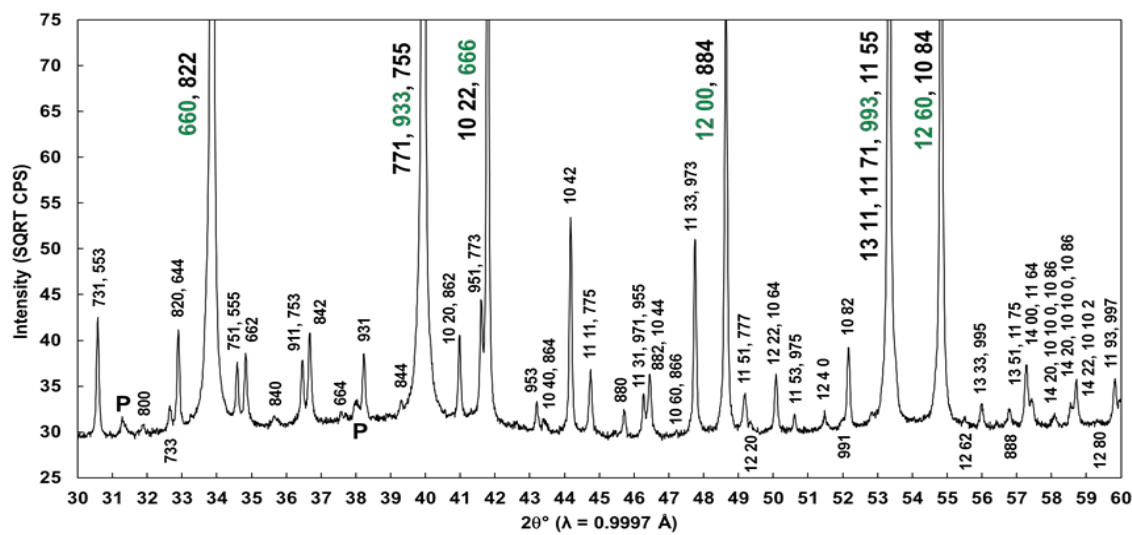
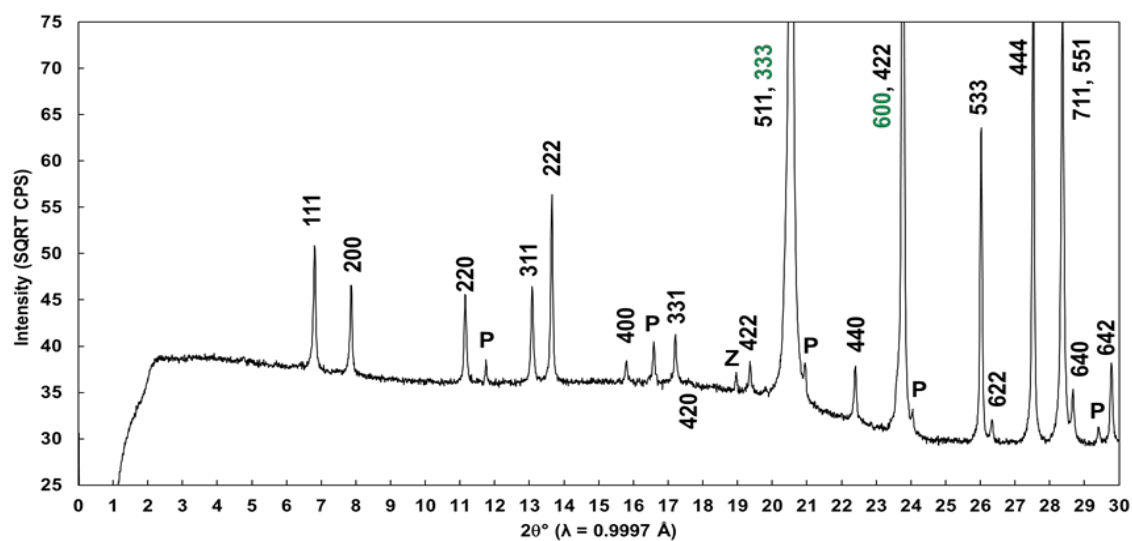


Fig. S2. The HAADF-STEM image in the (110) plane of the CTZAF sample. The FFT pattern in the (110) plane of the reciprocal lattice is shown inset.



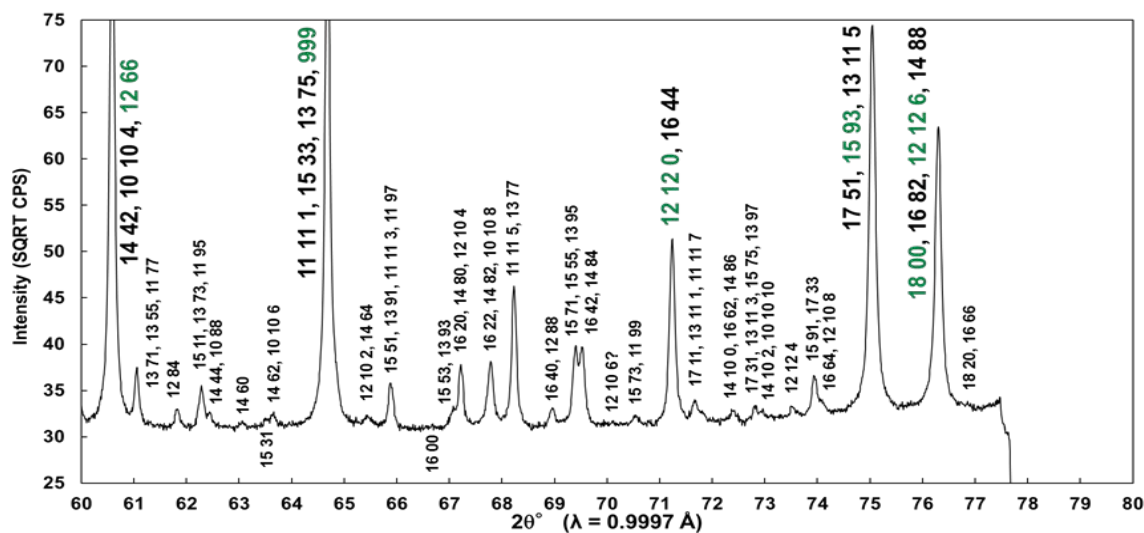


Fig. S3. Expanded synchrotron PXRD patterns of CMTZAF with minor impurities: P, pseudobrookite and Z, zirconolite. The SPXRD result of CMTZAF clearly produced the strong peaks from $3 \times (hkl)$ of the FCC sub-cell and many overlapping diffractions because of high symmetries (as here with FCC).

Simulation

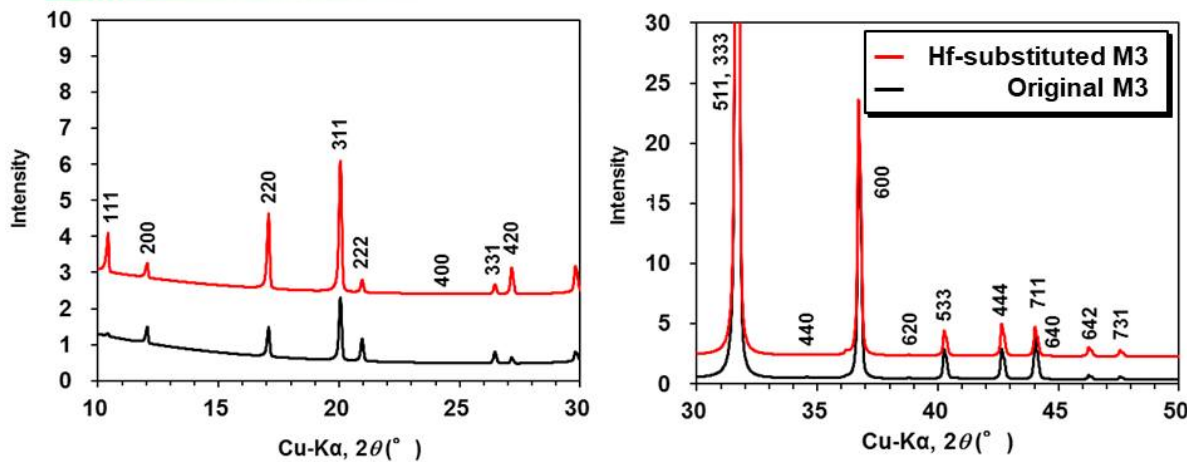


Fig. S4. The simulated pattern with the replacement of $[^6]TiI$ site (substitution of Hf for Zr ion at TiI site with [6]-coordination).

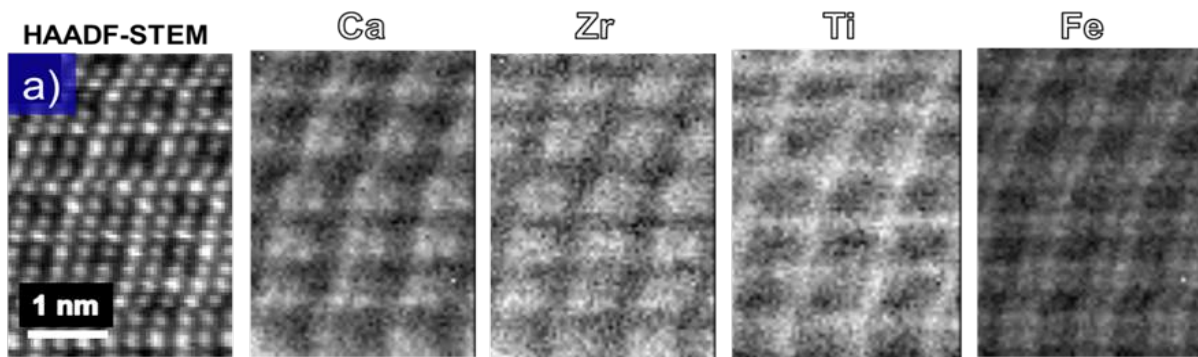


Fig. S5. The HAADF-STEM image (a) and STEM-EELS maps showing the distribution of Ca, Zr, Ti and Fe ions from the simpler (Mn-free) M3 sample of CTZAF in the (110) plane.

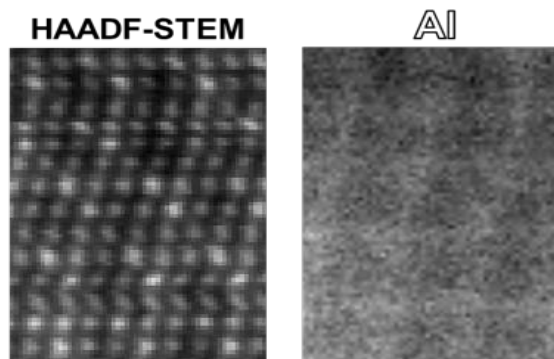


Fig. S6. The HAADF-STEM image and STEM-EELS map showing the distribution of Al from the simpler (Mn-free) M3 sample of CTZAF in the (110) plane.

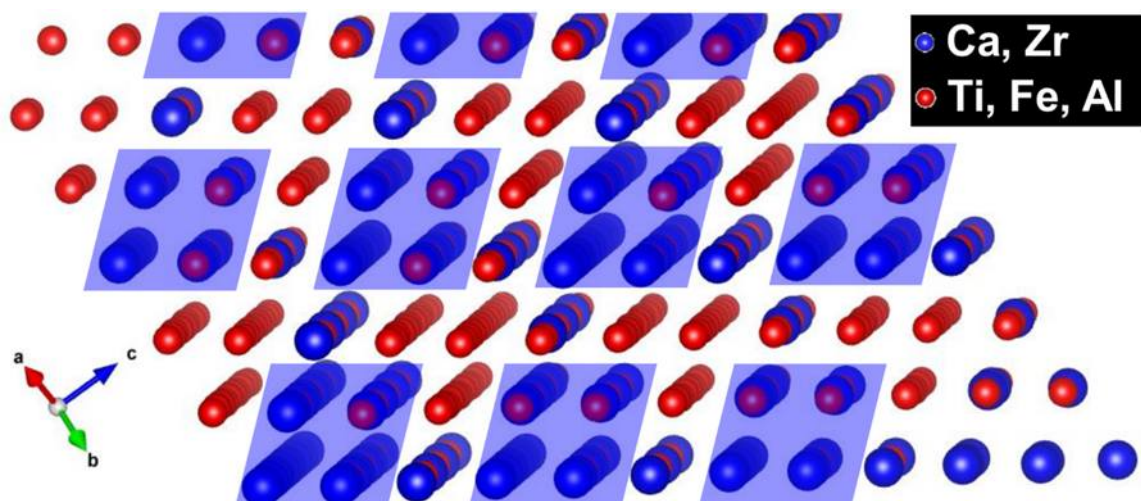


Fig. S7. The cation distribution in the structure model of M3 in the [110] direction: Ca and Zr at *Ca1* and *Ca2* site are with [8]-coordination, possibly now also [7]-; Ti at *Ti1* site are in [6]-coordination; Fe at *Ti2* site with [5]-coordination; Al at *Al* site is in [4]-coordination in $[8]CaI_6^{[8]}Ca2_4^{[6]}TiI_{12}^{[5]}Ti2_4^{[4]}AlO_{42}$.